Intramolecular Excimer Emission of Triply Bridged [3.3.*n*](3,6,9)Carbazolophanes

Hiroaki Benten, Hideo Ohkita, and Shinzaburo Ito*

Department of Polymer Chemistry, Graduate School of Engineering, Kyoto University, Katsura, Nishikyo, Kyoto 615-8510, Japan

Masahide Yamamoto

Faculty of Science and Engineering, Ritsumeikan University, Kusatsu, Shiga 525-8577, Japan

Naoki Sakumoto, Kazushige Hori, Yasuo Tohda, and Keita Tani

Division of Natural Science, Osaka Kyoiku University, Asahigaoka, Kashiwara, Osaka 582-8582, Japan

Yosuke Nakamura and Jun Nishimura

Department of Chemistry, Gunma University, Kiryu, Gunma 376-8515, Japan

Received: March 24, 2005; In Final Form: August 24, 2005

The photophysical properties of a series of triply bridged [3.3.*n*](3,6,9)carbazolophanes ([3.3.*n*]Cz, $n = 3$, 4, 5, 6) were studied as a model compound for a fully overlapped carbazole excimer. In these [3.3.*n*]Cz molecules, a plane angle of the two carbazole moieties changed systematically from nearly parallel to oblique, with increases in the length of the methylene chain *n* bridging at the 9-position of each carbazole ring. Absorption bands of [3.3.*n*]Cz showed the blue-shift and the splitting for $^1L_a \leftarrow {}^1A$ and $^1L_b \leftarrow {}^1A$ transition bands of the reference carbazole monomer, respectively. These spectral changes in [3.3.*n*]Cz were explained by Kasha's molecular exciton theory with the distance *r* and dihedral angle θ between the carbazole moieties in the ground state. In both liquid and glass matrixes, [3.3.*n*]Cz showed intramolecular excimer emission. The emission peak wavelength changed from 409 nm ($n = 6$) to 480 nm ($n = 3$) depending on *r* in the ground state. The dependence of the peak wavelength on *r* clearly showed that relative configurations of carbazole moieties in the ground state were preserved even in the excimer states. The smaller radiative rate of the excimer emission than the reference monomer was explained by the dimer symmetry of [3.3.*n*]Cz.

1. Introduction

An excimer is a molecular complex formed between a molecule in the excited state and a molecule in the ground state.[1−3] Various aromatic molecules form excimers in fluid solutions, liquids, crystals, and polymers. Excimer formation is attributed to two types of molecular interactions: exciton resonance and charge resonance.[1−3] The exciton resonance interaction is due to dipole−dipole interactions between a molecule in the excited state and a molecule in the ground state. This interaction is anisotropic and depends on the separation distance and relative orientation of the transition dipole on each aromatic moiety in the excimer. The charge resonance interaction is due to Coulombic interaction between positive and negative molecular ionic states. The excimer states are considered to be represented by a mixture of these two states.[1−4]

The ability of excimer formation, geometrical structure of the complex, and related photophysical properties have been widely studied by using bischromophoric compounds, in which two chromophoric groups are connected by a methylene chain.[5−14] Hirayama studied the formation of excimers for a variety of diphenyl and triphenyl alkanes in solutions and found that intramolecular excimers can be formed only when the two phenyl groups were separated by three carbon atoms ($n = 3$ rule).[5] Investigation of a series of dinaphthyl alkanes[6−8] and of 1,3-bis(*N*-carbazolyl)propane[9,10] generalized the $n = 3$ rule to these chromophores as well. The study of intramolecular excimers with a series of α,ω-di(1-pyrenyl)alkanes by Zachariasse and Kühnle essentially confirmed that the most stable excimer is a compound with three carbon atoms.[11] This rule suggests that the stability of intramolecular excimers in a solution is maximized when the two chromophoric groups can overlap in a sandwichlike geometry with their short and long in-plane molecular axes essentially parallel.

On the other hand, there are other types of excimers besides fully overlapped excimers.[15−21] Johnson proposed that there are two types of excimers in poly(*N*-vinylcarbazole).[15] One is the fully overlapped sandwich-type excimer and the other is a partially overlapped excimer (second excimer). Ito and coworkers studied the fluorescence properties in poly(3,6-di-*tert*-butyl-9-vinylcarbazole) and its sterically hindered dimeric model compounds and revealed that, even with small overlapping of aromatic planes, this polymer exhibits excimer emission.[20,21] These findings suggest that photophysical properties of aromatic excimers sensitively depend on the overlap of the two aromatic rings and their relative orientation.

These different types of excimers can be distinguished from each other by the polarization characteristics, the maximum wavelength of the fluorescence band, and the lifetime of the emissive state. However, such spectroscopic data do not provide

* Corresponding author. E-mail: sito@photo.polym.kyoto-u.ac.jp. Fax: +81-75-383-2617.

10.1021/jp051539s CCC: $30.25
Published on Web 09/29/2005

the details of the distance and mutual orientations of chromophores in the excimer. The formation of intramolecular excimers in bischromophoric molecules with a flexible linkage needs to change their conformation, which makes it difficult to discuss the relation between the excimer configuration and the characteristic photophysical properties. Therefore, model compounds with a rigid structure are desired to study the photophysical properties of excimers in terms of the geometrical configuration.

Cyclophane compounds have a unique structure in which two aromatic rings are aligned in face-to-face orientations by bridging with methylene chains.[22−26] Intramolecular excimer fluorescence is also observed in various cyclophanes (e.g., naphthalenophane,[27,38] anthracenophane,[29] pyrenophane,[30] phenanthrenophane,[31,32] carbazolophane[33,34]). Furthermore, paracyclophanes or multiple-bridged cyclophanes with more than two bridges would preserve the distance and mutual orientation of chromophores between the ground and excimer states owing to their rigid structure.[35] Therefore, cyclophane is an excellent model for studying the photophysical properties of excimers in terms of the geometrical alignments of two chromophores.[28,34]

Previously, we investigated the structure and photophysical properties of *syn*- and *anti*-[3.3](3,9)carbazolophanes and revealed that they are good model compounds of fully and partially overlapped carbazole excimers, respectively.[33,34] In the present study, we focus on the fully overlapped carbazole excimer. To discuss their photophysical properties in more detail, we synthesized a series of novel triply bridged [3.3.*n*](3,6,9)-carbazolophanes ([3.3.*n*]Cz, $n = 3, 4, 5, 6$) as a model compound for the fully overlapped carbazole excimer. These [3.3.*n*]Cz molecules have unique structures that the dihedral angle of two carbazole rings changes systematically from parallel to oblique with increases in the length of the methylene bridge *n*. On the basis of the well-defined rigid structure of [3.3.*n*]Cz molecules, we discussed the characteristic photophysical properties of the fully overlapped carbazole excimer depending on the separation distance and the dihedral angle formed between two carbazole rings.

2. Experimental Section

Materials. *Carbazolophanes and Reference Compounds.* *N*-Ethylcarbazole (EtCz) was synthesized by *N*-alkylation of carbazole and was purified by silica gel column chromatography and by recrystallization. 3,6-Dimethyl-*N*-ethylcarbazole (DMeCz) was prepared by the reduction of 3,6-bis(bromomethyl)-*N*-ethylcarbazole with $NaBH_4$. 1,3-Bis(3,6-dimethyl-*N*-carbazolyl)-propane (2DMeCz) was prepared from 1,3-bis(3,6-dibromomethyl-*N*-carbazolyl)propane and purified by recrystallization from ethanol.[36] [3.3.*n*](3,6,9)Carbazolophanes ([3.3.*n*]Cz, $n = 3, 4, 5, 6$) were synthesized by intramolecular cyclization of 1,3-bis(3,6-dibromomethyl-*N*-carbazolyl)alkane or 1,3-bis(3,6-dichloromethyl-*N*-carbazolyl)butane with NH_2CN. Details of the synthesis have been described elsewhere.[36] Chart 1 shows the chemical structures of the carbazole compounds used in this study.

Solvents. Solvents used here were tetrahydrofuran (THF, Nacalai Tesque, spectroscopic grade) and 2-methyl tetrahydrofuran (MTHF, Tokyo Kasei). Tetrahydrofuran was used without further purification. Prior to use, MTHF was dried with solid KOH, passed through freshly activated alumina, and then distilled from CaH_2 with 2,6-di-*tert*-butyl-*p*-cresol.

Poly(methyl methacrylate) Glass Samples. Methyl methacrylate monomer (MMA, Nacalai Tesque) was washed with a 5% NaOH aqueous solution twice and with a 20% NaCl aqueous solution four times, dried by Na_2SO_4 for 1 day, and then distilled under reduced pressure. Poly(methyl methacrylate) (PMMA) glass samples doped with the carbazolophanes were prepared in a Pyrex cell by the bulk polymerization of degassed MMA by using the 2,2′-azobisisobutyronitrile (AIBN, Wako) as an initiator. Concentration of carbazolophanes and AIBN in MMA was on the order of 10^{-5} mol L^{-1} and 5×10^{-4} mol L^{-1}, respectively. Polymerization was done at 60 °C for 17 h and at 70 °C for 13 h.

CHART 1: Chemical Structure of *N*-Ethylcarbazole (EtCz), 3,6-Dimethyl-*N*-ethylcarbazole (DMeCz), 1,3-Bis(3,6-dimethyl-*N*-carbazolyl)propane (2DMeCz), and [3.3.*n*](3,6,9)Carbazolophane ([3.3.*n*]Cz)

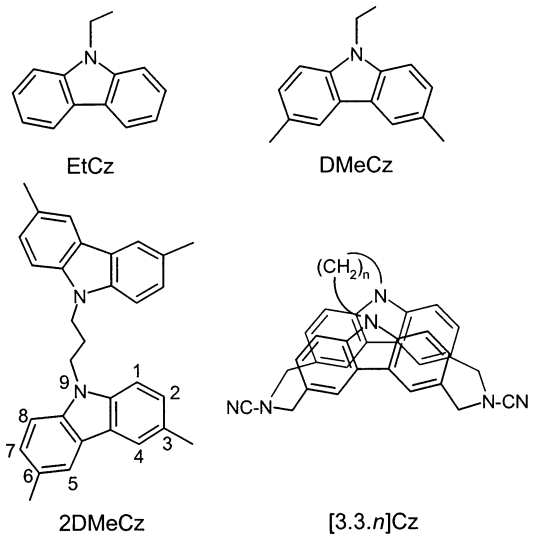

Absorption and Fluorescence Measurements. Steady-state absorption and emission spectra were measured at room temperature in a 1 cm quartz cell with a spectrophotometer (Hitachi, U-3500) and a fluorescence spectrophotometer (Hitachi, F-4500), respectively. Samples in the MTHF and THF solvent were degassed by the freeze−pump−thaw method and by Ar bubbling for 30 min, respectively. The concentration of carbazole compounds was on the order of 10^{-5} mol L^{-1}.

Fluorescence Polarization Measurements. The polarization of the fluorescence for PMMA glass samples was measured at room temperature. The degree of polarization *P* was calculated by the following equation:

$$P(\lambda) = (I_{VV}(\lambda) - g(\lambda)I_{VH}(\lambda))/(I_{VV}(\lambda) + g(\lambda)I_{VH}(\lambda))$$

where I_{XY} is the intensity of the emission that is measured when the excitation polarizer is in position X (V for vertical, H for horizontal), the emission polarizer is in position Y. Here, $g(\lambda) = I_{HV}(\lambda)/I_{HH}(\lambda)$ is a correction factor for the polarization of the apparatus used.

Fluorescence Decay Measurements. Fluorescence decay was measured by the time-correlated single-photon-counting method. Details have been described elsewhere.[34]

Results and Discussion

Structures of [3.3.*n*](3,6,9)Carbazolophanes. The structures of [3.3.*n*]Cz ($n = 3, 4, 5, 6$) molecules have been determined by X-ray analyses.[36] Two carbazole rings completely overlap each other for all [3.3.*n*]Cz molecules regardless of the length of the methylene chain bridging two carbazole moieties at their 9-position. On the other hand, a dihedral angle θ formed between two carbazole rings increases with increases in the

TABLE 1: Geometrical Parameters Determined by X-ray Analyses and Exciton Band Splitting Energy ΔE of ^1L_b Monomer Band

	r_A[a] (Å)	r_{N-N}[b] (Å)	r_{CC}[c] (Å)	r_B[d] (Å)	θ (deg)	ΔE (cm^{-1})
[3.3.3]Cz	3.46	3.31	3.48	3.15	2.7	2345
[3.3.4]Cz	4.00	4.14	3.65	3.20	17.2	1658
[3.3.5]Cz	4.65	4.96	3.89	3.32	30.6	1492
[3.3.6]Cz	4.68	5.02	3.88	3.30	33.1	1322

[a] The average distance between two carbon atoms at 1-position and 8-position in each carbazole ring. [b] The distance between the nitrogen atoms at 9-position in each carbazole ring. [c] The definition of r_{CC} is shown in Figure 1. [d] The average distance between two carbon atoms at 3-position and 6-position in each carbazole ring.

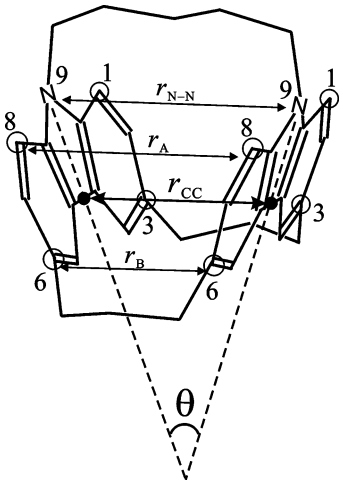

Figure 1. Mutual orientation of carbazole moieties in [3.3.*n*]Cz and definition of geometrical parameters r_A, r_{N-N}, r_{CC}, r_B, and θ.

methylene chain length. Geometrical parameters of [3.3.*n*]Cz determined by the X-ray analyses are listed in Table 1; the definition of the parameters are shown in Figure 1. The dihedral angle θ increases from 2.7 to 33.1° with the increase in the methylene chain length at 9-position. Both r_A and r_{N-N} increase with the increase in the methylene chain length at 9-position, while r_B was almost constant owing to the bridging chains at 3- and 6-positions. These results clearly show that mutual orientation of the carbazole moieties in a dimer varies continuously depending on the length of the methylene chain bridging the two carbazole moieties at 9-position. On the basis of the well-defined geometry, photophysical properties of [3.3.*n*]Cz molecules are discussed in the following sections.

Absorption Spectra. Figure 2a shows the absorption spectra of 2DMeCz and [3.3.4]Cz in a THF solution at room temperature. The absorption bands of 2DMeCz at 300 and 356 nm were assigned to the $^1L_a \leftarrow {}^1A$ and $^1L_b \leftarrow {}^1A$ transitions of carbazole moieties, respectively.[37,38] The absorption spectra of 2DMeCz was just twice as large as the spectra of DMeCz, indicating that there is no electronic interaction between the two carbazole moieties of 2DMeCz in the ground state. On the other hand, absorption bands of [3.3.4]Cz were slightly shifted compared with those of 2DMeCz. The ^1L_a band of [3.3.4]Cz was blue-shifted from 300 to 293 nm, and the ^1L_b band was split into two bands at 342 and 362 nm. Compared with the monomer ^1L_b band at 356 nm, a split absorption band at 342 nm was larger, while the other split band at 362 nm was smaller. Similar changes in absorption spectra were observed for all [3.3.*n*]Cz (n = 3, 4, 5, 6) molecules. These findings indicate that the two carbazole moieties in [3.3.*n*]Cz electronically interact with each other in the ground state.

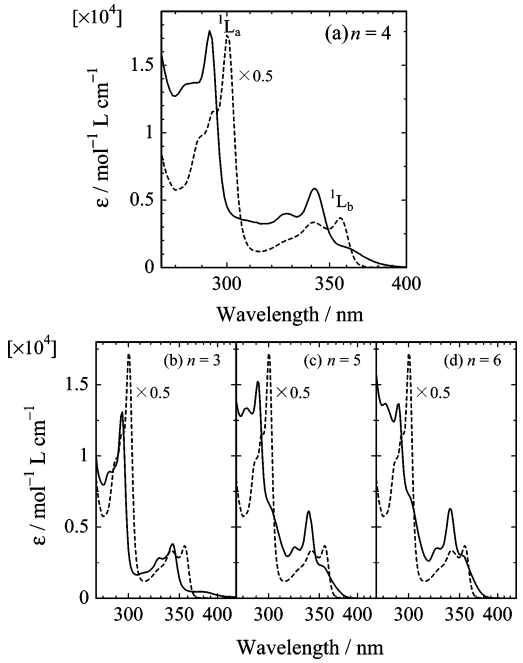

Figure 2. Absorption spectra of 2DMeCz (broken line) and [3.3.*n*]Cz (solid line) in a THF solution at room temperature: (a) [3.3.4]Cz, (b) [3.3.3]Cz, (c) [3.3.5]Cz, and (d) [3.3.6]Cz. The molar absorption coefficient ϵ of 2DMeCz is multiplied by a factor of 0.5.

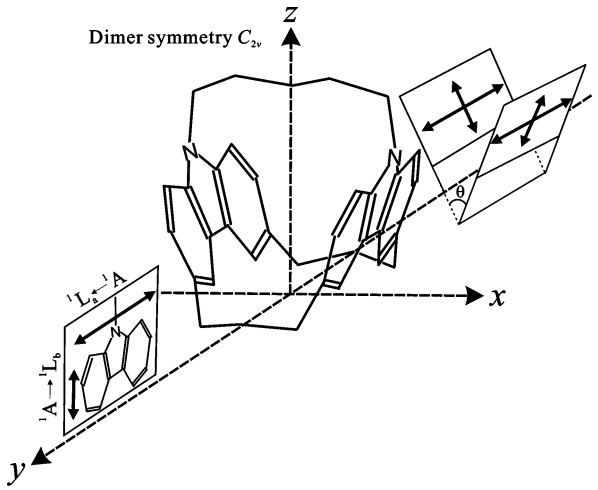

Figure 3. Coordinate system and alignments of transition dipole moments for both [3.3.*n*]Cz and a carbazole monomer. The $^1L_a \leftarrow {}^1A$ transition dipole moment of a carbazole monomer is polarized along the long molecular axis *y*. The $^1L_b \leftarrow {}^1A$ transition dipole moment is polarized along the short molecular axis *z*. The $^1L_a \leftarrow {}^1A$ transition dipole moments of carbazole moieties in [3.3.*n*]Cz exist along the *y* axis and are both parallel. The $^1L_b \leftarrow {}^1A$ transition dipole moments of carbazole moieties in [3.3.*n*]Cz are tilted $^1/_2\,\theta$ to the *z* axis and mutually oblique.

The peak shift observed in [3.3.*n*]Cz molecules can be qualitatively explained by the Kasha's exciton coupling theory.[39−42] The $^1L_a \leftarrow {}^1A$ transition dipole moment of a carbazole moiety is polarized along the long molecular axis *y*. The $^1L_b \leftarrow {}^1A$ transition dipole moment is polarized along the short molecular axis *z*. Figure 3 shows both the long (^1L_a) and short (^1L_b) transition dipoles of a carbazole moiety and the mutual orientation of the two carbazole moieties in [3.3.*n*]Cz. As shown in the figure, a long transition dipole of a carbazole moiety in [3.3.*n*]Cz is parallel to that of the other carbazole moiety. On the other hand, short transition dipoles in the tilted [3.3.*n*]Cz molecules are oblique with a mutual angle θ. Figure

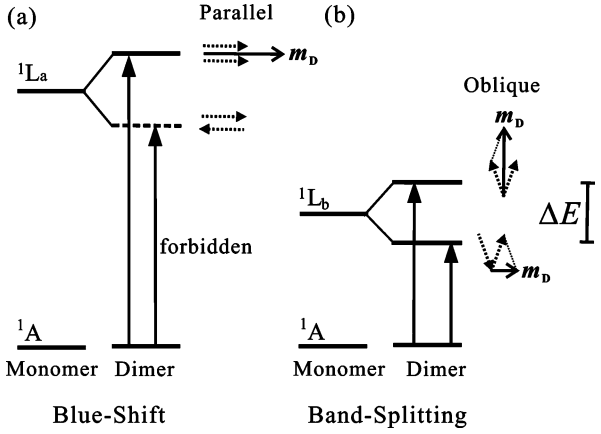

Figure 4. Diagrams for exciton band structure in a carbazole dimer taking tilted form. Transition dipoles polarized along the long molecular axis *y* of carbazole monomers are parallel arrangement (a), and those polarized along the short molecular axis *z* are oblique arrangement (b). The parallel and oblique dotted arrows represent transition dipoles of each carbazole monomer and the solid arrows $\boldsymbol{m}_D$ are the vector sum of the interacting monomer dipoles in the dimer. ΔE is the exciton splitting energy of the ^1L_b band, which corresponds to the same symbol ΔE in Figure 5a and is given by eq 1.

4 shows the energy diagram of exciton states and selection rules from the ground state to each exciton state for the tilted [3.3.*n*]-Cz molecules.[39,40] Owing to the electrostatic interaction of transition dipole moments in the carbazole moieties, each excited state is split into two exciton states. As for the ^1L_a band, two transition dipole moments interact electronically in a parallel arrangement. The out-of-phase interaction leads to the exciton state lower than the isolated excited state, and the in-phase interaction leads to the exciton state higher than the isolated excited state. The selection rule from the ground state to each exciton state depends on the dimer geometry; it can be deduced by the vector sum of the transition moments. Transition from the ground state to the lower exciton state (out-of-phase) is forbidden because the vector sum of the transition dipoles is equal to zero, while transition to the higher exciton state (in-phase) is allowed because the vector sum of the transition dipoles is twice as large as the transition dipole of an isolated molecule[43] (Figure 4a). Consequently, a blue-shift of the ^1L_a band results from these excitonic interactions along the long molecular axis *y* in [3.3.*n*]Cz. As for the ^1L_b band, on the other hand, two transition dipole moments interact electronically in an oblique arrangement. For the ^1L_b band, the in-phase interaction leads to the higher exciton state and the out-of-phase interaction leads to the lower exciton state. As illustrated in Figure 4b, the vector sum of the in-phase dipole moments is much larger than that of the out-of-phase dipole moments. Thus, the band-splitting of the ^1L_b band with different absorption intensity is also explained by the excitonic interactions along the short molecular axis *z* in [3.3.*n*]Cz.

For the discussion of the transition dipole moments of the ^1L_b band, polarization excitation spectra of [3.3.*n*]Cz molecules and DMeCz monomer were measured. Figure 5 shows the ^1L_b absorption bands of [3.3.*n*]Cz molecules and polarization excitation spectra of [3.3.5]Cz in a PMMA glassy solid at room temperature (circles) and in a MTHF liquid at room temperature (broken line) by monitoring at the emission maximum 414 nm, and the polarization excitation spectrum of DMeCz in a MTHF rigid glass at 77 K (solid line) at 385 nm. The polarization degree of the excitation spectrum was around zero for all [3.3.*n*]-Cz molecules in a MTHF liquid at room temperature. The polarization sign of DMeCz in a MTHF rigid glass remained

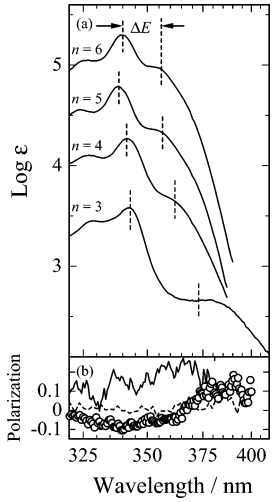

Figure 5. Exciton splitting of the ^1L_b band in [3.3.*n*]Cz molecules (a), and the polarization excitation spectra of [3.3.5]Cz and DMeCz (b). Absorption spectra of [3.3.4]Cz, [3.3.5]Cz, and [3.3.6]Cz are shifted along the longitudinal axis by a factor of $1 \times 10^{0.5}$. The polarization excitation spectra of [3.3.5]Cz were measured in a PMMA glass (circles) and in a MTHF liquid (broken line) at room temperature by monitoring at the emission maximum 414 nm, and of DMeCz in a MTHF glass at 77 K (solid line) at 385 nm.

positive in the whole wavelength range of the ^1L_b band. On the other hand, the polarization sign of [3.3.5]Cz in a PMMA glassy solid changed from negative to positive at a longer wavelength of the ^1L_b band. This polarization change was also observed for all [3.3.*n*]Cz molecules. These findings are consistent with the assignments described above; the transition dipole moment from the ground state to the higher exciton state of ^1L_b is perpendicular to that from the ground state to the lower exciton state of ^1L_b. Furthermore, the negative polarization suggests that the transition dipole moment from the emissive state to the ground state is perpendicular to that from the ground state to the higher exciton state of ^1L_b, and the positive polarization suggests that the transition dipole moment from the emissive state to the ground state is parallel to that from the ground state to the lower exciton state of ^1L_b.

Next, the exciton splitting energy of the ^1L_b band is discussed on the basis of the geometrical parameters of [3.3.*n*]Cz. As shown in Figure 5a, the exciton splitting energy ΔE of the ^1L_b band increased with the decrease in the length of the 9-bridged methylene chain (Table 1). These systematic spectral changes were also explained by the Kasha's exciton coupling theory.[39,40] According to the theory, the exciton splitting energy ΔE owing to the dipole−dipole interaction is given by eq 1,

$$\Delta E = 2\frac{|\boldsymbol{M}|^2}{4\pi\epsilon_0}\frac{(\cos\theta + 3\cos\alpha\cos\beta)}{r^3} \qquad (1)$$

where ϵ_0 is the vacuum permittivity and $\boldsymbol{M}$ is the transition dipole moment of the monomer. The definition of angles θ, α, β, and the separation distance between centers of the dipoles *r* are given in Figure 6. Assuming that α and β are equal to $(180° - \theta)/2$, eq 1 is simplified to eq 2:

$$\Delta E = 2\frac{|\boldsymbol{M}|^2}{4\pi\epsilon_0}\frac{(1 + \sin^2(\theta/2))}{r^3} = |\boldsymbol{M}|^2 f(\theta,r) \qquad (2)$$

Here r_{CC}, which is defined in Figure 1, was used as *r* of oblique dipoles on the two carbazole moieties in [3.3.*n*]Cz. As shown in Figure 7, the experimental exciton splitting energy ΔE was

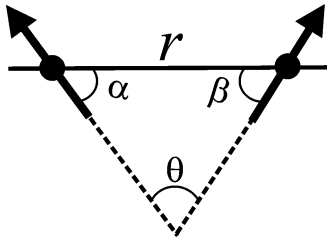

Figure 6. Oblique arrangement of two transition dipole moments (thick arrows).

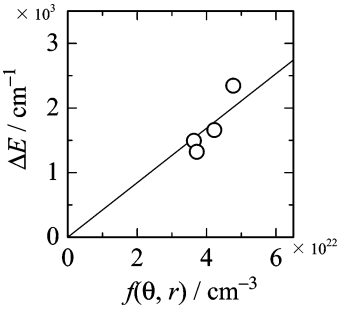

Figure 7. The exciton splitting energy ΔE plotted against the $f(\theta, r)$. In this calculation, r_{CC} was used as the separation distance r between centers of the oblique transition dipoles polarized along the short molecular axis on the carbazole moieties.

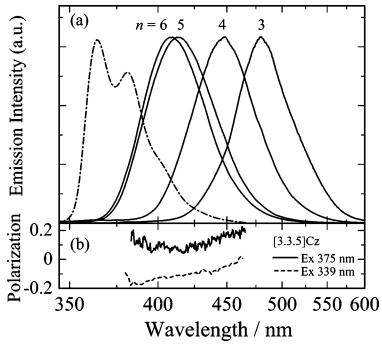

Figure 8. Fluorescence spectra of 2DMeCz (dashed−dotted line) and [3.3.*n*]Cz molecules (solid lines) in a THF solution at room temperature (a), and the polarization emission spectra of [3.3.5]Cz upon 339 nm excitation (broken line) and 375 nm excitation (solid line) in PMMA glass at room temperature (b). The peak wavelength of the excimer fluorescence is 409 nm ($n = 6$), 414 nm ($n = 5$), 448 nm ($n = 4$), and 480 nm ($n = 3$), respectively. Emission intensity was normalized.

linearly proportional to the calculated $f(\theta, r)$. From the slope, $\boldsymbol{M}$ was evaluated to be 2.9 D. This is comparable to the value (ca. 2.2 D) estimated from both oscillator strength and peak wavelength associated with the ^1L_b band of the carbazole monomer.[44,45] Consequently, it is concluded that the exciton splitting energy can be understood by the geometrical parameters of [3.3.*n*]Cz, mutual orientation and distance of transition dipole moments, in the framework of the Kasha's exciton coupling theory.

Fluorescence Spectra. Figure 8a shows the fluorescence spectra of 2DMeCz (dashed−dotted line) and [3.3.*n*]Cz molecules (solid lines) in THF at room temperature. The fluorescence spectrum of 2DMeCz was clearly ascribed to the DMeCz monomer, which had vibrational bands at 364 and 382 nm. On the other hand, the fluorescence spectra of [3.3.*n*]Cz molecules showed only a red-shifted broad emission band without a vibrational structure. These broad emissions were also observed even in a MTHF rigid matrix at 77 K where translational diffusion is negligible. Excitation spectra of [3.3.*n*]Cz molecules were the same as the corresponding absorption spectra. Therefore, these findings show that the broad structureless emission of [3.3.*n*]Cz molecules is not ascribed to any impurities but to intramolecular excimer fluorescence. The peak shift from the ^1L_b band of the monomer absorption of 2DMeCz corresponded to 3640 cm^{-1} for [3.3.6]Cz, 3935 cm^{-1} for [3.3.5]Cz, 5768 cm^{-1} for [3.3.4]Cz, and 7257 cm^{-1} for [3.3.3]Cz in energy. The large Stokes shift and spectral change in the emission spectra are characteristic of most aromatic excimers, suggesting that medium interaction between two carbazole moieties in the ground state due to dipole−dipole interaction changes to strong interaction in the excited state due to both exciton and charge resonance interaction leading to excimer formation.

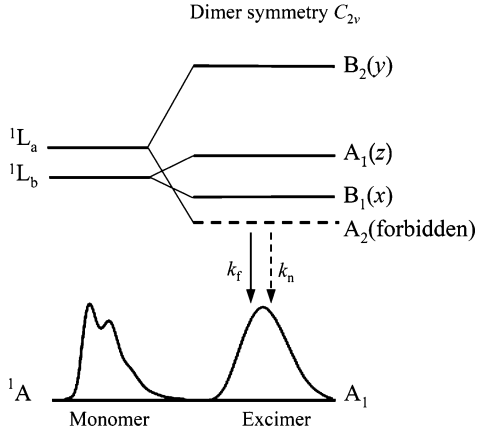

Figure 9. Energy level diagrams of carbazole dimer in C_{2v} symmetry and symmetry species for each energy level. The notations of *x*, *y*, *z* in parentheses show the polarization of the transitions between the corresponding states and the ground state.

The large red-shift of the excimer emission in [3.3.*n*]Cz molecules and its *n* dependence arise from the stabilization of the emissive state due to both exciton and charge resonance interactions and from the ground-state destabilization due to the electronic repulsion between carbazole rings. The charge resonance interaction and the ground-state destabilization are caused by the overlap between the orbitals of adjacent atoms in the different carbazole rings. With the decrease in the methylene chain length *n* in [3.3.*n*]Cz molecules, the orbital overlap becomes larger, which leads to the stabilization of the emissive state by the effective charge resonance interaction and also to the destabilization in the ground state by the electronic repulsion. In particular, the destabilization in the ground state will be largest in the [3.3.3]Cz because the average separation distance between the carbazole rings is 3.35 Å, which is slightly shorter than an interplanar distance of 3.40 Å of aromatic nuclei packed in a crystal lattice.[46] These interactions lead to the larger red-shift of excimer emission observed in [3.3.*n*]Cz molecules with smaller *n*. In addition to these two interactions owing to the overlap between the electronic wave functions of carbazole rings, the exciton resonance interaction plays an important role in the large red-shift of excimer emission in [3.3.*n*]Cz molecules and its *n* dependence. Here, we focus on the exciton resonance interaction and discuss the experimental results based on the exciton theory.

According to the theoretical prediction,[4,47] the lowest energy excimer state is the ^1L_a lower exciton resonance state, which lies below the ^1L_b exciton resonance states because of the relatively strong transition dipole moment along the molecular long axis. Figure 9 shows the energy diagram of a fully overlapped carbazole excimer proposed.[15] Because relative orientation of the long molecular axis is parallel for all [3.3.*n*]-Cz molecules, the stabilization of the excimer state by the exciton interaction depends on the separation distance *r* ac-

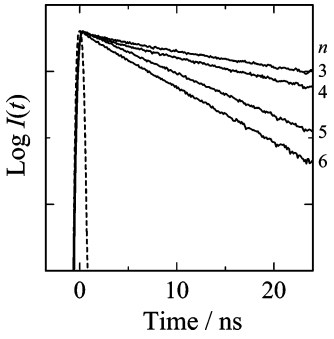

Figure 10. Fluorescence decay curves of [3.3.*n*]Cz molecules in a MTHF solution at room temperature. Excitation wavelength was 295 nm for all samples. Monitor wavelength were 479 nm ($n = 3$), 445 nm ($n = 4$), 413 nm ($n = 5$), and 408 nm ($n = 6$) for [3.3.*n*]Cz, respectively. The broken line shows an excitation laser pulse.

TABLE 2: Fitting Parameters for Fluorescence Decay, Fluorescence Quantum Yield Φ_f, Radiative Rate k_f, and Nonradiative Rate k_n, of EtCz and [3.3.*n*]Cz ($n = 3, 4, 5, 6$) Molecules in a MTHF Solution at Room Temperature

	τ_1 (ns)	τ_2 (ns)	A_1	A_2	χ^2	Φ_f	k_f (s^{-1})	k_n (s^{-1})
EtCz[a]	14.4		1.0		1.27	0.43	3.0×10^7	4.0×10^7
[3.3.3]Cz	37.1	2.3	0.89	0.11	1.43	0.040	1.1×10^6	2.6×10^7
[3.3.4]Cz	26.5	2.0	0.88	0.12	1.44	0.044	1.6×10^6	3.6×10^7
[3.3.5]Cz	13.8	2.4	0.94	0.06	1.02	0.054	3.9×10^6	6.9×10^7
[3.3.6]Cz	10.6	0.77	0.88	0.12	1.29	0.068	6.4×10^6	8.8×10^7

[a] Taken from ref 34.

cording to r^{-3}. Thus, the excimer state is more stable as the number n is smaller. The continuous peak shift to longer wavelength can be roughly explained by the molecular exciton interaction between the ^1L_a transition dipole moments, which increases with decreasing n. In other words, the conformation of excimer is similar to that of the ground state because of their restricted conformation of triply bridged [3.3.*n*]Cz, even though there exists a strong interaction in the excimer state.

Figure 8b shows the polarization emission spectra of [3.3.5]-Cz in a PMMA glassy solid at room temperature excited at 339 nm (broken line) and at 375 nm (solid line), which correspond to the higher and lower exciton state of the ^1L_b band, respectively. The polarization sign was negative for the excitation at 339 nm and positive for the excitation at 375 nm. The same tendency was observed for other [3.3.*n*]Cz molecules. These findings ensure that the transition dipole moment from the excimer to the ground state is perpendicular to that from the ground to the higher exciton state of the ^1L_b band and it is parallel to that from the ground to the lower exciton state of the ^1L_b band.

Fluorescence Decay Measurements. To examine the excimer state of [3.3.*n*]Cz ($n = 3, 4, 5, 6$) molecules, the fluorescence decay was measured in the MTHF solution. As shown in Figure 10, no fluorescence rise was observed for any sample within the instrument response function (ca. 750 ps). This finding indicates that excimer formation in [3.3.*n*]Cz molecules is completed faster than 750 ps after laser excitation and requires just a slight conformational change. The fluorescence decays were fitted to the following equation consisting of two exponential terms by the nonlinear least-squares method:

$$I(t) = I_0\{A_1 \exp(-t/\tau_1) + A_2 \exp(-t/\tau_2)\} \qquad (3)$$

The fitting parameters are summarized in Table 2. The radiative rates, k_f, in Table 2 are ascribable to those of the intramolecular excimers of [3.3.*n*]Cz molecules because there was no monomer emission in the steady-state emission spectra of the carbazolophanes and there was no rise in the fluorescence decays. The radiative rates of [3.3.*n*]Cz molecules were smaller than that of EtCz (3.0×10^7 s^{-1}),[34] while the nonradiative rates, k_n, were on the same order. These slow radiative rates show that excimer emissions of [3.3.*n*]Cz molecules are partially forbidden. According to theoretical prediction, the polarization of transitions between these excited states and the ground state is derived as shown in Figure 9 (in parentheses) for the dimer in C_{2v} symmetry.[15] The selection rule in the group theory predicts that the lowest-lying A_2 state of the dimer is not dipole-coupled to the ground A_1 state. Therefore, the excimer fluorescence of [3.3.*n*]Cz in C_{2v} symmetry is ascribed to a forbidden transition from the excited A_2 state to the ground A_1 state. The value of k_f was about 1/30 smaller for [3.3.3]Cz and about $^1/_5$ smaller for [3.3.6]Cz than that of EtCz. The increase in k_f with increasing n shows that the conformation in the excimer state becomes slightly flexible for [3.3.*n*]Cz with a large n. The deviation from a strict C_{2v} symmetry results in a partially dipole-allowed character from the lowest excited state to the ground state.

4. Conclusion

The photophysical properties of triply bridged [3.3.*n*](3,6,9)-carbazolophanes ([3.3.*n*]Cz, $n = 3, 4, 5, 6$) were studied as a model compound for a fully overlapped carbazole excimer. Although all [3.3.*n*]Cz molecules take a face-to-face configuration, their electronic properties varied sensitively, reflecting the structural differences in the ground state. Absorption spectra showed a slight change compared with the fluorescence spectra. The change was explained by Kasha's molecular exciton theory. The blue-shift of the ^1L_a band results from the fully overlapped parallel orientation of the transition dipoles along the long molecular axis. The splitting and its width of the ^1L_b band can be explained by considering both the separation distance and the angle between the transition dipoles along the short molecular axis. Fluorescence spectra showed only the excimer emission. The emission peak shifted sensitively, reflecting the difference in the separation distance of carbazole rings in the ground state. The lifetime of excimer emissions varied sensitively by the slight increase in the flexibility of [3.3.*n*]Cz. The smaller radiative rates k_f, however, showed that excimer state configuration remains almost the same as that in the ground-state being in the symmetry C_{2v}. Owing to the well-defined rigid structures of [3.3.*n*]Cz, we can discuss the characteristic photophysical properties of the fully overlapped carbazole excimer depending on the separation distance and the dihedral angle formed between two carbazole rings.

References and Notes

(1) Birks J. B. *Photophysics of Aromatic Molecules*; Wiley-Interscience: London, 1970.
(2) Birks J. B. *Rep. Prog. Phys.* **1975**, *38*, 903.
(3) Barashkov, N. N.; Sakhno, T. V.; Nurmukhametov, R. N.; Khakhel′, O. A. *Russ. Chem. Rev.* **1993**, *62*, 539.
(4) McGlynn, S. P.; Armstrong, A. T.; Azumi, T. In *Modern Quantum Chemistry, Part III*; Sinanoğlu, O., Ed.; Academic Press: New York, 1965; p 203.
(5) Hirayama, F. *J. Chem. Phys.* **1965**, *42*, 3163.
(6) Chandross E. A.; Dempster, C. J. *J. Am. Chem. Soc.* **1970**, *92*, 3586.
(7) Ito, S.; Yamamoto, M.; Nishijima, Y. *Bull. Chem. Soc. Jpn.* **1981**, *54*, 35.
(8) Ito, S.; Yamamoto, M.; Nishijima, Y. *Bull. Chem. Soc. Jpn.* **1982**, *55*, 363.
(9) Klöpffer, W. *Chem. Phys. Lett.* **1969**, *4*, 193.
(10) Klöpffer, W. *J. Chem. Phys.* **1969**, *50*, 2337.
(11) Zachariasse K.; Kühnle, W. *Z. Phys. Chem. N. F.* **1976**, *101*, 267.

(12) Hayashi, T.; Suzuki, T.; Mataga, N.; Sakata, Y.; Misumi, S. *Chem. Phys. Lett*. **1976**, *38*, 599.
(13) Johnson, G. E. *J. Chem. Phys*. **1974**, *61*, 3002.
(14) Itagaki, H.; Obukata, N.; Okamoto, A.; Horie, K.; Mita, I. *Chem. Phys. Lett*. **1981**, *78*, 143.
(15) Johnson, G. E. *J. Chem. Phys*. **1975**, *62*, 4697.
(16) Itaya, A.; Okamoto, K.; Kusabayashi, S. *Bull. Chem. Soc. Jpn*. **1976**, *49*, 2082.
(17) De Schryver, F. C.; Vandendriessche, J.; Toppet, S.; Demeyer, K.; Boens, N. *Macromolecules* **1982**, *15*, 406.
(18) Vandendriessche, J.; Palmans, P.; Toppet, S.; Boens, N.; De Schryver, F. C.; Masuhara, H. *J. Am. Chem. Soc*. **1984**, *106*, 8057.
(19) Itagaki, H.; Obukata, N.; Okamoto, A.; Horie, K.; Mita, I. *J. Am. Chem. Soc*. **1982**, *104*, 4469.
(20) Ito, S.; Takami, K.; Tsujii, Y.; Yamamoto, M. *Makromol. Chem., Rapid Commun*. **1989**, *10*, 79.
(21) Ito, S.; Takami, K.; Tsujii, Y.; Yamamoto, M. *Macromolecules* **1990**, *23*, 2666.
(22) Cram D. J.; Cram, J. M. *Acc. Chem. Res.* **1971**, *4*, 204.
(23) Ferguson, J. *Chem. Rev*. **1986**, *86*, 957.
(24) Masuhara, H.; Mataga, N.; Yoshida, M.; Tatemitsu, H.; Sakata, Y.; Misumi, S. *J. Phys. Chem*. **1977**, *81*, 879.
(25) Otsubo, T.; Kitasawa, M.; Misumi, S. *Bull. Chem. Soc. Jpn*. **1979**, *52*, 1515.
(26) Yasutake, M.; Koga, T.; Sakamoto, Y.; Komatsu, S.; Zhou, M.; Sako, K.; Tatemitsu, H.; Onaka, S.; Aso, Y.; Inoue, S.; Shinmyozu, T. *J. Am. Chem. Soc*. **2002**, *124*, 10136.
(27) Froines J. R.; Hagerman, P. J. *Chem. Phys. Lett*. **1969**, *4*, 135.
(28) Yanagidate, M.; Takayama, K.; Takeuchi, M.; Nishimura, J.; Shizuka, H. *J. Phys. Chem*. **1993**, *97*, 8881.
(29) Morita, M.; Kishi, T.; Tanaka, M.; Tanaka, J.; Ferguson, J.; Sakata, Y.; Misumi, S.; Hayashi, T.; Mataga, N. *Bull. Chem. Soc. Jpn*. **1978**, *51*, 3449.
(30) Hayashi, T.; Mataga, N.; Umemoto, T.; Sakata, Y.; Misumi, S. *J. Phys. Chem*. **1977**, *81*, 424.
(31) Nakamura, Y.; Tsuihiji, T.; Mita, T.; Minowa, T.; Tobita, S.; Shizuka, H.; Nishimura, J. *J. Am. Chem. Soc.* **1996**, *118*, 1006.
(32) Nishimura, J.; Nakamura, Y.; Hayashida, Y.; Kudo, T. *Acc. Chem. Res*. **2000**, *33*, 679.
(33) Tani, K.; Tohda, Y.; Takemura, H.; Ohkita, H.; Ito, S.; Yamamoto, M. *Chem. Commun*. **2001**, 1914.
(34) Ohkita, H.; Ito, S.; Yamamoto, M.; Tohda, Y.; Tani, K. *J. Phys. Chem. A* **2002**, *106*, 2140.
(35) Benten, H.; Ohkita, H.; Ito, S.; Yamamoto, M.; Tani, K.; Tohda, Y. *Bull. Chem. Soc. Jpn*. **2004**, 77, 393.
(36) Tani, K.; Sakumoto, N.; Kubono, K.; Hori, K.; Tohda, Y.; Benten, H.; Ohkita, H.; Ito, S.; Yamamoto, M. *Chem. Commun.* to be submitted.
(37) Platt, J. R. *J. Chem. Phys*. **1949**, *17*, 484.
(38) Johnson, G. E. *J. Phys. Chem*. **1974**, *78*, 1512.
(39) Kasha, M. *Radiat. Res.* **1963**, *20*, 55.
(40) McRae, E. G.; Kasha, M. In *Physical Process in Radiation Biology*; Augenstein, L., Mason, R., Rosenberg, B., Ed.; Academic Press: New York, 1964.
(41) The criteria for exciton coupling strength in the dimer is proposed by Simpson and Peterson in ref 42, where the coupling strength is defined by the ratio of $2V/\Delta$. The term $2V$ is the exciton bandwidth and the other Δ is the Franck−Condon bandwidth of the corresponding molecular electronic transition in the individual molecular unit. In our carbazolophanes, $2V$ of the ^1L_b band is about 2300 cm^{-1} for the [3.3.3]Cz and about 1500 cm^{-1} for other [3.3.*n*]Cz ($n = 4, 5, 6$), and Δ of the monomer ^1L_b absorption (fwhm) is about 3200 cm^{-1}. According to these values, the exciton interaction in [3.3.*n*]Cz ($n = 3, 4, 5, 6$) is not in the strong coupling range, satisfying the relation of $(2V/\Delta) \gg 1$, but in the intermediate coupling range. Although the Kasha's molecular exciton theory is applicable to the strong coupling case, in this report, the theory is used to explain the spectral shifts in [3.3.*n*]Cz under the assumption that it is valid for the intermediate coupling.
(42) Simpson, W. T.; Peterson, D. L. *J. Chem. Phys*. **1957**, *26*, 588.
(43) The transition dipole moment from the ground state to the higher exciton state of ^1L_a is the square root of two times larger than that from the ground state to the ^1L_a state of an isolated molecule.
(44) Transition dipole moment of the $^1L_b \leftarrow {}^1A$ band for the carbazole monomer $\boldsymbol{M}$ was calculated by using the equation $f = (8\pi^2 m_e)/(3he^2)\, \nu\, |\boldsymbol{M}|^2$, where f is the oscillator strength, ν the frequency in Hz for the absorption maximum, m_e the mass of an electron, h the Planck's constant, e the elementary charge. The coefficient $(3he^2)/(8\pi^2 m_e)$ is 7.095×10^{-43} $m^2\ s^{-1}\ C^2$. For *N*-methyl carbazole, $\boldsymbol{M}$ was calculated to be 2.2 D in cyclohexane by using the data, $f(S_1 - S_0) = 0.067$ and the absorption maximum wavelength $\lambda_{max}(abs) = 344$ nm, which were listed in ref 45.
(45) Bonesi, S. M.; Balsells, R. E. *J. Lumin*. **2001**, *93*, 51.
(46) Robertson J. M. *Organic Crystals and Molecules*; Cornell University Press: Ithaca, NY, 1953.
(47) Azumi, T.; Armstrong, A. T.; Mcglynn, S. P. *J. Chem. Phys.* **1964**, *41*, 3839.